Models for Frequency Doppler Shift Prediction for LEO Satellites at L-Band

Omid Nia
ECE Dept., George Mason University, Fairfax, VA, U.S.A.
Iridium Communications, McLean, VA, U.S.A.

Brian L. Mark
Dept. of Electrical and Computer Engineering
George Mason University, Fairfax, VA, U.S.A.

***Abstract*—In low-earth-orbit (LEO) satellite communications, frequency Doppler shift (FDS) results in lower or higher received frequency than the signal initially transmitted from the satellite. To maintain high throughput and low bit error rate, FDS compensation methods are needed. Such methods rely on the accurate prediction of FDS. In this paper, we study and evaluate four models for frequency Doppler shift prediction in the LEO constellation at L-Band frequency using both simulation and experimental measurements from the Iridium NEXT constellation. Two models are from the literature and two new models are introduced here. The two new models differ from the existing models by estimating the earth's central angle using multiple factors, i.e., the slant ranges for different elevation angles and the coordinates of both the satellite and the earth station. Our simulation and experimental results confirm that the new models achieved significantly improved accuracy in various scenarios.**

***Index Terms*—SATCOM, LEO constellation, L-Band, Doppler shift, Iridium NEXT.**

I. Introduction

Many low-earth-orbit (LEO) satellites have been launched, and more will be established for broadband communication in the next couple of years. The LEO satellites offer several advantages over medium-earth-orbit (MEO) and geostationary orbit (GEO) satellites, including higher received signal power and lower latency. Moreover, LEO satellites are deployed in individual constellations and communicate in different frequency bands, which provides spectral diversity.

One of the most challenging problems in LEO satellites is accurately estimating the down-link frequency for Doppler shift analysis. A frequency Doppler shift (FDS) occurs when a source of waves moves relative to an observer or vice versa, resulting in a change in frequency in relation to the observer. These Doppler shifts must be compensated for in satellite communications to deliver the most accurate and reliable services. Frequency Doppler shift prediction (FDSP) is a possible solution to help the ground transceivers compensate for the Doppler shift errors. A Doppler estimation scheme using the relative time information was introduced in [1] and [2]; these authors consider the simple case of circular LEO satellites in the equatorial plane and Doppler observed by points on the equator. Figure 1 shows the effects of four orbital passes, as a series of S-shaped curves, for four different frequency types (i.e., 144 MHz in VHF, 433 MHz in UHF, 1.6 GHz (L-band), and 2.4 GHz in UHF).

In this paper, we study four models for FDSP based on LEO satellites with circular (or elliptical) orbits. The first

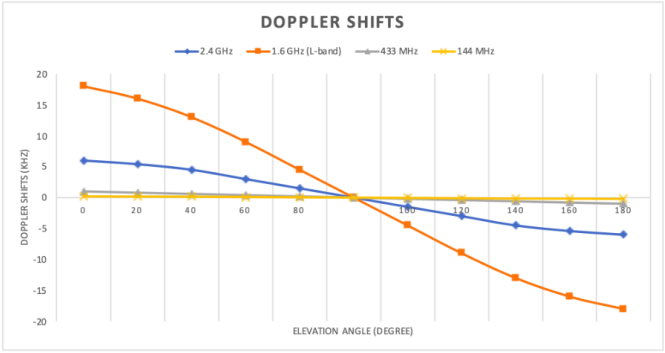

Fig. 1: Doppler shifts based on the elevation angles (LEO: orbit $H = 780$ km) with the fixed ground station.

two models, referred to as Model I and Model II, are from the literature [2] and [3], while the other two, referred to as Model III and Model IV, are original models developed in this paper. The baseline model, Model I, achieves low range error in lower orbit but incurs a substantial prediction error variance in other scenarios such as higher altitudes, weak signal environments, or different geographical areas. The two new models introduced in this paper, Models III and IV, use different input values observed at the maximum elevation angle, inclination, the ground station coordinate, and the earth terminal coordinates and may reduce the FDSP error in different scenarios. We compare the four models using both simulations via the Systems Tool Kit (STK) and experimental measurements from the Iridium NEXT satellite constellation. We conclude that one of the new models, Model IV, is the most promising approach for FDSP, achieving the lowest error margins.

The remainder of the paper is organized as follows. Section II describes the orbital model and assumptions for LEO that are used to evaluate the proposed FDSP models. Section III develops the four FDSP models in detail and compares them using STK simulation. In Section IV, we present experimental results obtained from measurements of the Iridium NEXT network and use them to evaluate the four FDSP models. Concluding remarks are given in Section V.

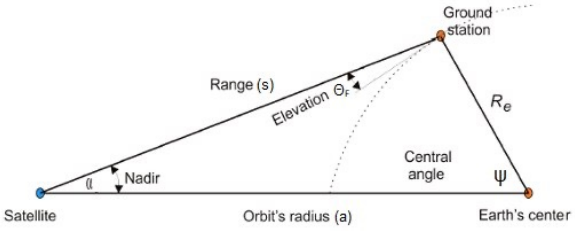

Fig. 2: Ground station geometry.

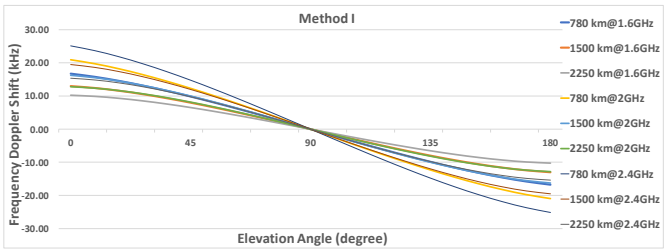

Fig. 3: Model I simulation results (f_{DM1}).

II. Orbital Model and Assumptions

Low Earth orbits are between 300–3000 km in altitude. They are characterized by the orbital velocity needed to maintain the satellite in orbit, about 7.5 km/s in the lowest orbits. As described in [4], the orbital period is about 90 minutes due to this high velocity, which means that a satellite is in view for only a few minutes. The FDS is present in the communication links because of the relative velocity between the satellite and any particular point on the Earth. In most cases, this FDS must be compensated for by the earth terminal equipment.

The slant range (s) represents the distance between a satellite and a ground station. This range changes over time. The altitude (a) or orbital's radius can be calculated as

$$H + R_e = a, \tag{1}$$

where R_e is the Earth's radius (6378 km) and H is the LEO satellite's height from the ground. The angle formed between the ideal horizon plane and the slant range is called the elevation angle, θ_F. The LEO satellite orbit is parameterized on the maximum elevation angle observed at the earth station. The earth is considered to be spherical and lower-order perturbations are ignored.

III. Frequency Doppler Shift Prediction Models

Figure 2 shows the ground stationary geometry. Two sides of the triangle in the figure are known: the distance R_e from the ground station to the earth's center and the distance a from the satellite to earth's center-orbital radius. There are four critical variables in this triangle: the elevation angle θ_F; the central angle ψ, i.e., the separation angle between the satellite and the earth terminal; the slant range s; and the nadir angle α, which is the angle under which the satellite sees the ground station. Given two of these variables, the others can be found using the following equations [5]:

$$\alpha + \theta_F + \psi = 90, \tag{2}$$

$$s \cos\theta_F = a \sin\psi, \tag{3}$$

$$s \sin\alpha = R_e \sin\psi, \tag{4}$$

In FDS prediction, the critical parameter is the slant range s. This parameter is used during the link budget calculation and is expressed through the elevation angle θ_F. Applying the cosine law to the triangle in Fig. 2 yields

$$s(t) = \sqrt{a^2 + {R_e}^2 - 2aR_e \cos\psi(t)}. \tag{5}$$

Our objective is to predict the FDS $f_D(t)$ as accurately as possible based on the variables $\psi(t)$ and $\theta_F(t)$. From the frequency Doppler fundamental, we can define the FDS equation relative to the frequency of the carrier, f_c, the velocity of the satellite, and the speed of light c as follows:

$$f_D(t) = f_c \frac{v(t)}{c}, \tag{6}$$

Since the frequency shift produced by the Doppler effect is proportional to the relative velocity between transmitter and receiver, the momentum of the satellite can be obtained as the derivative of the slant range $s(t)$ between the satellite and the station:

$$v(t) = -\frac{ds(t)}{dt}, \tag{7}$$

Inserting (5) into (7), and then applying the result to (6) yields the following generic equation for FDS prediction:

$$f_D(t) = \frac{f_c}{c} \frac{aR_e}{s(t)} \frac{d\cos\psi(t)}{dt}, \tag{8}$$

The $\cos\psi(t)$ term can be derived in two different ways as discussed below.

A. Baseline Model: Model I

We use the FDSP model in [6] as a baseline and refer to it as Model I. Based on the horizon angle in t_0 using the angular momentum, t_0 is the period at the satellite making the maximum elevation angle with the earth station in the earth-centered, earth-fixed coordinate system. Consequently, $\theta_F(t_0)$ is the maximum elevation angle at t_0, a known angle based on the geographical area and the satellite inclination angle θ_i. As was done in [3], using the elevation angle between the earth station and the satellite, we can write the central angle as

$$\cos\psi(t) = \cos(\theta_F(t) - \theta_F(t_0)) \cos\psi(t_0). \tag{9}$$

Estimation of the term $\psi(t_n)$ with Model I is dependent on $\psi(t_0)$. Error in the estimation of $\psi(t_0)$ propagates to estimates of $\psi(t_1), \psi(t_2), \ldots, \psi(t_n)$, which could cause a significant error in the prediction process. From Fig. 2, we have

$$\cos(\theta_F(t) - \psi(t_0)) = (r/a) \cos(\theta_F(t)). \tag{10}$$

We can then derive

$$\cos\psi(t_0) = \cos^{-1}((r/a)\cos\theta_F(t)) - \theta_F(t_0)). \tag{11}$$

Substituting (11) into (9) results in

$$\cos\psi(t) = g(t)\cos(\theta_F(t) - \theta_F(t_0)), \tag{12}$$

where

$$g(t) = \cos\left(\cos^{-1}((r/a)\cos\theta_F(t)) - \theta_F(t_0)\right). \tag{13}$$

Substituting (12) into (8), we obtain the following equation for the Model I FDS prediction:

$$f_{\mathrm{DM1}}(t) = \frac{f_c}{c}\frac{aR_e}{s(t)}\frac{d\cos\psi(t)}{dt} \tag{14}$$

$$= \frac{f_c aR_e \sin(\theta_F(t) - \theta_F(t_0))\ g(t)\frac{d\cos\theta_F(t)}{dt}}{c\sqrt{a^2 + R_e^2 - 2aR_e\cos(\theta_F(t) - \theta_F(t_0))g(t)}}. \tag{15}$$

From the angular momentum fundamental, we have

$$\frac{d\cos\theta_F(t)}{dt} = \omega_F(t) = \omega_s - \omega_e\cos\theta_i, \tag{16}$$

where ω_s is the angular velocity of the moving satellite, ω_e is the angular velocity of the earth terminal, and θ_i is the satellite inclination angle. We derive a simpler expression for $f_{\mathrm{DM1}}(t)$ by substituting (16) into (15):

$$f_{\mathrm{DM1}}(t) = \frac{f_c}{c}\frac{aR_e}{s(t)}\frac{d\cos\psi(t)}{dt} = \frac{f_c aR_e \sin(\theta_F(t) - \theta_F(t_0))g(t)(w_s - w_e\cos\theta_i)}{c\sqrt{a^2 + {R_e}^2 - 2aR_e\cos(\theta_F(t) - \theta_F(t_0))\ g(t)}}. \tag{17}$$

Figure 3 shows a simulated S-shaped variation for maximum elevation angles $\theta_F(t_0)$ ranging over 0, 15, and 25 degrees for a hypothetical terminal with six different altitude and frequency configurations using Model I. All simulations were done with the Systems Tool Kit (STK) software. The simulated symmetric S-curve graph follows the pattern in Fig. 1, which verifies Model I. The Model I simulation reports the FDS range between +20 to -20 kHz with a 780 km satellite height and at 1.6 GHz with a maximum elevation $\theta_F(t_0)$ of 15 degrees.

Ali et al. [7] have proposed using the Model I FDSP method in LEO constellations. Elias [8] proposed using the algorithm published by Ali et al. to predict the maximum elevation using Model I. A more recent paper by Zizhong et al. [9] also presented experimental results based on accurate Iridium data collected in a weak signal environment under a dense forest at Beijing University of Aeronautics and Astronautics (BUAA) for 30 minutes. The actual measured FDS shown in [9, Fig. 9a] lines up with the simulated data in this paper as shown in Fig. 3. Zizhong et al. measured insubstantial error margin [8] and actual frequency Doppler shift results in the field.

B. Alternative Existing Model: Model II

The second model, referred to as Model II, is from [3] and is based on the coordinates of a fixed earth terminal and instantaneous LEO satellite position. We have

$$\cos\psi(t) = \cos T_s(t)\cos T_e\cos(G_s(t) - G_e) + \sin T_s(t)\sin T_e, \tag{18}$$

where $T_s(t)$ is the latitude of the moving satellite at time t, $G_s(t)$ is the longitude of the moving satellite, T_e is the earth terminal's latitude, and G_e is the longitude of the earth terminal. We derive $f_{\mathrm{DM2}}(t)$ by substituting (18) into (5) and (8), and considering the second derivative of $\cos\psi(t)$ as follows:

$$\frac{d^2\cos\psi(t)}{dt^2} = -w_F^2(t)\cos\psi(t). \tag{19}$$

We then obtain

$$f_{\mathrm{DM2}}(t) = \frac{f_c}{c}\frac{aR_e}{s(t)}\frac{d\cos\psi(t)}{dt} = \frac{h(t)}{c\sqrt{u(t)}}, \tag{20}$$

where

$$u(t) = a^2 + R_e^2 - 2aR_e\big(\cos T_s(t)\cos T_e\cos(G_s(t) - G_e) + \sin T_s(t)\sin T_e\big), \tag{21}$$

and

$$h(t) = f_c a_e\left\{\left[-w_s\sin\theta_i\cos\left(\sin^{-1}\left(\frac{\sin T_s(t)}{\sin\theta_i}\right)\right)\cdot\tan T_s(t)\cos(G_s(t) - G_e) - \left(\frac{w_s\cos\theta_i}{\cos T_s(t)} - w_e\cos T_s(t)\right)\cdot\sin(G_s(t) - G_e)\right]\right\}\cos T_e + w_s\sin\theta_i\cos T_s(t)\sin T_e. \tag{22}$$

Figure 4 shows the STK simulation analysis of the S-shaped variation for a hypothetical terminal connecting to six different altitude and frequency configurations using Model II.

As shown in Figure 4, regardless of the operating frequencies, the FDS in Model II merges 10-20 degrees before and after the satellite converges to the overhead elevation. Theoretically, based on (8), Doppler shifts should not merge unless the satellite is over the pinnacle angle. The simulated S-curve graph for Model II does not follow the pattern (Fig. 1). The Model II simulation reports the FDS range between +35 to -35 kHz at 780 km height and 1.6 GHz frequency.

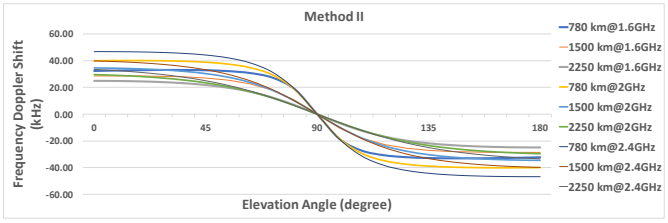

Fig. 4: Model II simulation results (f_{DM2}).

C. Proposed Models: Model III and Model IV

Model I uses the relative time to the reference time when the satellite makes the "maximum elevation angle" with the user terminal. The algorithm is limited in this scenario, which can conclude this low error range. The prediction algorithm based on Model I produces an FDS with a significant prediction error variance in other scenarios with features such as higher altitudes, weak signal environments, or different geographical areas. Considering the L-band communication operation, the prediction error tolerance is essential for statistical reasons and the instantaneous time. New prediction methods using satellite

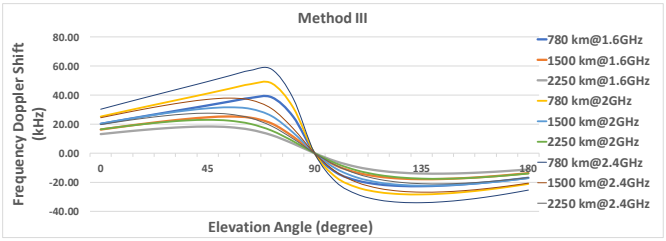

Fig. 5: Model III simulation results (f_{DM3}).

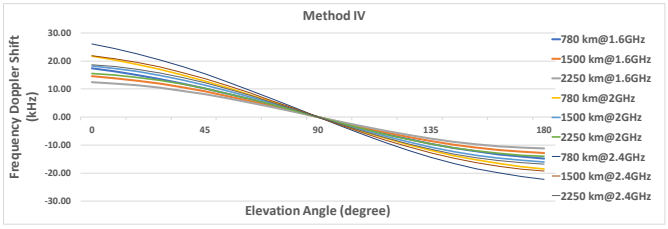

Fig. 6: Model IV simulation results (f_{DM4}).

and stationary ground station parameters are proposed to reduce prediction error. We propose the new Models III and IV, which use the value observed at the maximum elevation angle, the ground station, and the earth terminal coordinates. The new methods can improve the terminal's ability in weak signal Doppler estimation or different altitudes to obtain a better error rate than Model I since more factors are considered. We will simulate the output of new models and compare them with Models I and II.

From (5), it is evident that the denominators in (17) and (20) are equal to the slant range s. Thus, the denominators can be swapped, which yields Model III:

$$f_{\mathrm{DM3}}(t) = \frac{f_c}{c}\frac{aR_e}{s(t)}\frac{d\cos\psi(t)}{dt} = \frac{f_c a R_e \sin(\theta_F(t)-\theta_F(t_0))g(t)(w_s - w_e\cos\ \theta_i)}{c(\theta_F(t)/10)\sqrt{u(t)}}, \quad (23)$$

where R_e is the Earth's radius, a is the LEO satellite's altitude (1), ω_s is the angular velocity of the moving Satellite, ω_e is the angular velocity of the earth terminal, and θ_i is the satellite inclination angle.

Figure 5 shows the simulated S-shaped variation for a hypothetical terminal communicating to six different altitude and frequency configurations using Method III. Equation (23) is based on the elevation in the numerator and uses the satellite and ground station coordinates in the denominators. In the denominator, $\theta_F(t)$ is the elevation angle where, for the negative FDS, 180 - $\theta_F(t)$ shall be used. Simulation of this method shows some anomalous results for shorter satellite altitudes (e.g., 780 km height) with different frequencies. The Model III simulation reports the FDS range between +20 to -10 kHz at a satellite height of 780 km satellite's and frequency 1.6 GHz with a maximum elevation $\theta_F(t_0)$ of 15 degrees.

Next, we derive another model, Model IV, as follows:

$$f_{\mathrm{DM4}}(t) = \frac{f_c}{c}\frac{aR_e}{s(t)}\frac{d\cos\psi(t)}{dt} = \frac{h(t)\theta_F(t)(1000/a)}{c\sqrt{a^2 + {R_e}^2 - 2aR_e\cos(\theta_F(t)-\theta_F(t_0))g(t)}}. \quad (24)$$

Using Model IV, Fig. 6 shows the simulated S-shaped variation for a hypothetical terminal connecting to six different altitude and frequency configurations. Equation (24) is based on the satellite's view elevation in the denominators and uses the numerator's satellite and ground station coordinates. The coordinates used for the Model IV prediction are the same as those used in Model II. Model IV simulation reports the FDS range between +20 to -20 kHz, at 780 km satellite height and 1.6 GHz with a maximum elevation angle $\theta_F(t_0)$ of 15 degrees. The angle $\theta_F(t)$ in the denominator is the elevation angle, where for negative FDS, $180-\theta_F(t)$ shall be used. Theoretically, the adaptive compensation algorithm (f_{DM4}) seems to be the most applicable alternative method for the LEO satellite systems for the general error tolerance level between 250-500 Hz. The Iridium constellation is approximately 780 kilometers (485 miles) above the Earth.

IV. Experimental Results and Evaluation

The Iridium NEXT constellation consists of 66 active LEO satellites that orbit the Earth in 6 different orbital planes spaced 30° apart. The planes are near-polar orbits with 86.4° inclination angle and 780 km orbital altitude. Iridium NEXT signals are transmitted over the 1616–1626.5 MHz band, part of the L-band. There are 252 carriers in both the up-link and down-link channels with carrier spacing of 41.6667 kHz, as discussed, for example, in [10].

A. Experimental Setup

The Iridium signals are functional in 30 duplex sub-bands between 1616 and 1626 MHz and 12 simplex channels between 1626 and 1626.5 MHz, which consist of 90 ms time-division multiple access (TDMA) frames. This paper employs random traffic channels throughout the Iridium NEXT carriers during the data ping burst using the 8.8.8.8 IP address, Google's primary Domain Name Service (DNS) server. Thus, in this test, we did not rely on the Ring channel only.

We next describe the ground terminal setup and downlink measurements and analyze the frequency Doppler measurements, which will be used to compare the four FDSP models discussed in Section III. The Iridium NEXT data were collected by a Thales VesseLINK 700 terminal installed on top of the Iridium headquarters building in McLean, VA (38.924, -77.223), for three different sweeps (about 15 minutes each). In contrast, different visibilities to the Iridium NEXT satellite were monitored for different angles of elevations (see Figure 6). In order to listen to the channels on the downlink only, two circulators were used and the output was obtained to measure the received signal's frequency with a vector signal analyzer.

No. of sats.	No. of planes	Inclin. °	Height (km)	Orbital Period (min)	Freq. Range (MHz)
66	6	86.4	781	100	1616–1626.5

TABLE I: Specifications of Iridium LEO satellite.

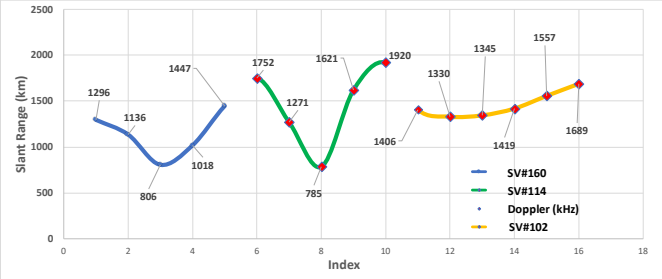

Fig. 7: Slant Ranges in km.

SV-160 (°N,°W)	Time @032922	Slant (km)	El.	Az.	FDS (kHz)
(30.1, 77.2)	11:28:45 AM	1296	32°	181°	26.65
(31.9, 77.2)	11:29:15 AM	1136	44°	181°	23.95
(37.2, 77.1)	11:30:45 AM	806	74°	183°	8.32
(44.4, 76.8)	11:32:45 AM	1018	65°	1°	-12.92
(49.2, 76.5)	11:34:45 PM	1427	28°	1°	-33.33
SV-114 (°N,°W)	Time @032922	Slant (km)	El.	Az	FDS (kHz)
(25.5, 76.7)	12:32:00 AM	1752	14°	178°	26.03
(34.8, 76.7)	12:33:30 AM	1271	63°	178°	18.02
(39.1, 76.5)	12:35:55 AM	785	85°	57°	0.82
(50.9, 75.8)	12:39:15 AM	1621	21°	3°	-30.43
(53.7, 75.5)	12:40:00 AM	1920	15°	3°	-36.05
SV-102 (°N,°W)	Time @032922	Slant (km)	El.	Az	FDS (kHz)
(34.8, 65.3)	13:46:30 PM	1406	34°	107°	21.87
(41.1, 65.2)	13:47:35 PM	1330	82°	84°	-0.63
(44.8, 65.1)	13:48:00 PM	1345	55°	73°	-15.63
(48.2,65)	13:48:45 PM	1419	28°	59°	-24.50

TABLE II: FDS for three different satellite positions.

B. Experimental Results

One set of results was captured on March 8, 2022, and two were conducted on March 29 (see Table II). Visible registered satellites were observed and recorded using some Python codes by extracting them from the recorded Wireshark (pcap) files. Later, all information was post-processed and linked to the measured values. Three Iridium NEXT satellites were visible and provided service to the VesseLINK Terminal on two different days and three trials, as listed in Table II. Satellite Vehicle identifiers were 160 (NORAD ID:43569), 114 (NORAD ID:41923), and 102 (NORAD ID:41920). Detailed coordinates are listed in Table II. In another view, all three satellite routes are referenced to the stationary terminal. Two of the satellites (SV-160 and SV-114) passed almost directly overhead (75° and 85° elevation angle in order), and the third satellite (SV-102) passed far away east on the Atlantic Ocean.

Every diamond point in Fig. 9 denotes the Doppler shift measured by subtracting the actual frequency from the expected frequency. Generally, the Doppler shift curve of the Iridium NEXT satellite is a kind of S-shape curve where we experience the lowest frequency Doppler when the satellite is in its lowest slant range or highest elevation angle (close to zero means the satellite is located near the top of the receiver). Figure 7 illustrates the slant ranges between the terminal and the visible satellite under test while moving very fast in the LEO constellation with about 7.5 km/s velocity, which also can

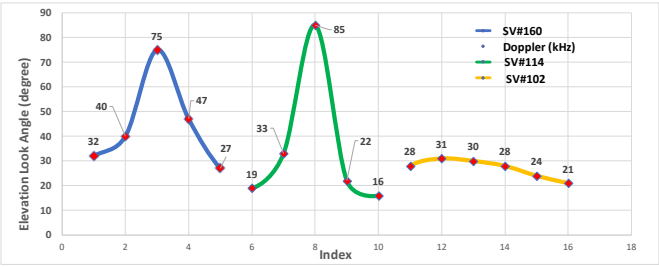

Fig. 8: Elevation look angles.

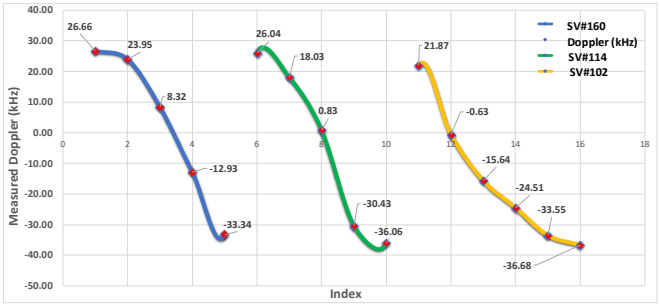

Fig. 9: Measured FDS in kHz.

be correlated to Fig. 8. The measured parameters in Table II and the graphs fall into the expected values, including the FDS versus elevation versus the slant range.

C. Evaluation of FDSP Models

In this section, we compare real-world experimental measurements with the FDSP results obtained using Models I–IV, i.e., f_{DM1} to f_{DM4}. This outcome rests on the distinction that whereas experiments are versions of the real-world captured, models are artificially constructed to represent the real world. Table III shows the FDS measurements and lists the calculated frequency Doppler shifts based on the four models, as shown on the right side of the table. The table is divided into three parts, where each part represents a different space vehicle (SV) with IDs: 160, 114, and 102. We compare our measurements to the FDS values calculated from the four models. Due to communication systems sensitivity, the Doppler frequency prediction error is given by

$$E_X(t) = f_{\mathrm{D}}(t) – f_{\mathrm{DMX}}(t), \tag{25}$$

where $X = 1, 2, 3, 4$. Table IV shows the Doppler frequency prediction errors $E_X(t)$. As can be observed, in most instances (slant range, elevation angles, and satellite coordinates), Model IV shows better performance compared to the other models with respect to the prediction error. Table IV shows the magnitudes of the prediction errors averaged over

SV-160 (°N,°W)	Slant (km)	El.	FDS (kHz)	f_{DM1} (kHz)	f_{DM2} (kHz)	f_{DM3} (kHz)	f_{DM4} (kHz)
(30.1, 77.2)	1296	32°	26.65	29.96	29.16	23.78	29.34
(31.9, 77.2)	1136	44°	23.95	27.28	26.57	21.97	26.35
(37.2, 77.1)	806	74°	8.32	11.03	9.37	9.77	8.45
(41.9, 76.8)	1018	65°	-12.92	-16.78	-14.55	-15.13	-12.88
(49.2,76.5)	1427	28°	-33.33	-29.92	-30.12	-22.6	-31.85
SV-114 (°N,°W)	Slant (km)	El.	FDS (kHz)	f_{DM1} (kHz)	f_{DM2} (kHz)	f_{DM3} (kHz)	f_{DM4} (kHz)
(25.5,76.7)	1752	14°	26.03	30.36	32.68	20.94	28.8
(34.8,76.7)	1271	63°	18.02	23.63	19.64	15.35	18.38
(39.1,76.5)	785	85°	0.82	4.6	-0.36	2.86	-0.35
(50.9,75.8)	1621	21°	-30.43	-36.96	-31.07	-21.70	-32.17
(53.7,75.5)	1920	15°	-36.05	-31.63	-32.31	-19.2	-32.35
SV-102 (°N,°W)	Slant (km)	El.	FDS (kHz)	f_{DM1} (kHz)	f_{DM2} (kHz)	f_{DM3} (kHz)	f_{DM4} (kHz)
(34.8,65.3)	1406	34°	21.87	23.94	18.22	20.69	20.93
(41.1,65.2)	1330	82°	-0.63	4.47	-0.30	2.72	-0.50
(44.8,65.1)	1345	55°	-15.63	-17.94	-10.85	-12.64	-15.37
(48.2,65)	1419	28°	-22.50	-23.94	-17.98	-19.21	-22.37

TABLE III: Measured frequency Doppler shift versus Models I-IV.

SV-160 (°N,°W)	Slant (km)	El.	$E_1(t)$ (kHz)	$E_2(t)$ (kHz)	$E_3(t)$ (kHz)	$E_4(t)$ (kHz)
(30.1,77.2)	1296	32°	-3.31	-2.51	2.87	-2.69
(31.9,77.2)	1136	44°	-3.33	-2.62	1.98	-2.4
(37.2,77.1)	806	74°	-2.71	-1.05	-1.45	-0.13
(41.9,76.8)	1018	65°	3.86	1.63	2.21	-0.04
(49.2,76.5)	1427	28°	-3.41	-3.21	-10.73	-1.48
SV-114 (°N,°W)	Slant (km)	El.	$E_1(t)$ (kHz)	$E_2(t)$ (kHz)	$E_3(t)$ (kHz)	$E_4(t)$ (kHz)
(25.5,76.7)	1752	14°	-4.33	-6.65	5.09	-2.77
(34.8,76.7)	1271	63°	-5.61	-1.62	2.67	-0.36
(39.1,76.5)	785	85°	-3.78	1.18	-2.04	1.17
(50.9,75.8)	1621	21°	6.53	0.64	-8.73	1.74
(53.7,75.5)	1920	15°	-4.42	-3.74	-16.85	-3.7
SV-102 (°N,°W)	Slant (km)	El.	$E_1(t)$ (kHz)	$E_2(t)$ (kHz)	$E_3(t)$ (kHz)	$E_4(t)$ (kHz)
(34.8°,65.3°)	1406	34°	-2.07	3.65	1.18	0.94
(41.1°,65.2°)	1330	82°	-5.1	-0.33	-3.35	-0.13
(44.8°,65.1°)	1345	55°	2.31	-4.78	-2.99	-0.26
(48.2°,65°)	1419	28°	1.44	-4.52	-3.29	-0.13

TABLE IV: Doppler frequency prediction error ($E_X(t)$).

fourteen scenarios. The averaged magnitudes of the prediction errors, denoted by $\overline{E}_X(t)$, $X = 1, 2, 3, 4$, are shown in Table V.

$\overline{E}_1(t)$	$\overline{E}_2(t)$	$\overline{E}_3(t)$	$\overline{E}_4(t)$
3.73 kHz	2.72 kHz	4.67 kHz	1.28 kHz

TABLE V: Average Doppler frequency prediction error ($\overline{E}_X(t)$) for Models I-IV, Iridium band and SV height 780 km.

V. Conclusion

More accurate FDSP will help LEO ground transceivers perform better frequency compensation against the phase distortion due to Doppler shifts. Such frequency compensation has the potential to significantly improve the bit error rate (BER) and the Signal to Noise Ratio (SNR) (i.e., up to 3dB or 10-15 percent). We studied and evaluated four different models of FDS in the LEO constellation. Models I and II are existing models from [2] and [3], respectively, while Models III and IV were developed in this paper. The new models take into account more parameters than the earlier models and are expected to perform better over a more extensive range of scenarios.

We conducted an experimental analysis using real-world frequency Doppler shift measurements based on the Iridium NEXT constellation. The experimental results clearly showed that Model IV achieved the smallest average prediction error over a variety of different scenarios. Our measured results in this paper showed that Model IV provides more accurate FDS predictions, up to 2 or 3 kHz better on average compared with Models I and II. Therefore, Model IV is a promising candidate for FDSP and frequency Doppler compensation for transceivers operating in the LEO constellation and L-band frequencies.

References

[1] M. Katayama, A. Ogawa, and N. Morinaga, "Carrier Synchronization under Doppler Shift of the Nongeostationary Satellite Communication Systems," in *Proc. Singapore ICCS/ISITA '92*, 1992, pp. 466–470 vol.2.

[2] I. Ali, N. Al-Dhahir, and J. E. Hershey, "Doppler Characterization for LEO Satellites," *IEEE Trans. Commun.*, vol. 46, no. 3, pp. 309–313, 1998.

[3] M.-H. You, S.-P. Lee, and Y. Han, "Adaptive Compensation Method using the Prediction Algorithm for the Doppler Frequency Shift in the LEO Mobile Satellite Communication System," *ETRI journal*, vol. 22, no. 4, pp. 32–39, 2000.

[4] M. G. Morgan and J. M. Peha, *Science and Technology Advice for Congress*. Routledge, 2003.

[5] S. Cakaj, B. Kamo, V. Koliçi, and O. Shurdi, "The Range and Horizon Lane Simulation for Ground Stations of Low Earth Orbiting (LEO) Satellites," *Int. J. Commun. Netw. Syst. Sci.*, vol. 4, no. 9, pp. 585–589, 2011.

[6] I. Ali, N. Al-Dhahir, and J. Hershey, "Accurate Doppler Characterization for LEO Satellites," *GE CRD Rep. 97CRD058*, 1997.

[7] I. Ali, N. Al-Dhahir, J. E. Hershey, G. J. Saulnier, and R. Nelson, "Doppler as a New Dimension for Multiple Access in LEO Satellite Systems," *Int. J. Satell. Commun. Netw.*, vol. 15, pp. 269–279, 1997.

[8] E. Aboutanios, "Frequency Estimation for Low Earth Orbit Satellites," Ph.D. dissertation, University of Technology Sydney, 2002.

[9] Z. Tan, H. Qin, L. Cong, and C. Zhao, "Positioning Using Iridium Satellite Signals of Opportunity in Weak Signal Environment," *Electronics*, vol. 9, no. 1, p. 37, 2019.

[10] M. Orabi, J. Khalife, and Z. M. Kassas, "Opportunistic Navigation with Doppler Measurements from Iridium Next and Orbcomm LEO satellites," in *IEEE Aerospace Conference*, 2021, pp. 1–9.